East European Journal of Physics. **4.** 57-71 (2022)
DOI:10.26565/2312-4334-2022-4-04 ISSN 2312-4334

STUDY OF THE NUCLEAR STRUCTURE FOR SOME NUCLEI USING SELF-CONSISTENT RPA CALCULATIONS WITH SKYRME-TYPE INTERACTION†

Noor M. Kareem[a,*], Ali A. Alzubadi[a]
[a]*University of Baghdad, College of Science, Department of Physics*
**Corresponding Author: nour.mohammed1204a@sc.uobaghdad.edu.iq*
Received September 8, 2022; revised October 11, 2022; accepted October 25, 2022

In the present research, some static and dynamic nuclear properties of the closed-shell nuclei;^{58}Ni, ^{90}Zr, ^{116}Sn, and ^{144}Sm have been studied using the Random Phase Approximation (RPA) with different Skyrme parameterizations, particularly SyO-, Sk255, SyO+, SLy4, BSk17, and SLy5. In particular, in studies of static properties such as single-particle radial nuclear densities for neutrons, protons, mass, and charge densities with their corresponding root mean square (rms) radii, All the obtained results agreed well with the relevant experimental data. Concerning the dynamic nuclear properties such as, the excitation energy, transition density, and giant resonance modes for the excitation to the low-lying negative partite excited states 1^-, 3^-, 5^-, and 7^- have also been studied. The obtained results that estimates of RPA with Skyrme-type interactions are a good way to describe the properties of the structure of even-even, closed-shell nuclei.
Keywords. Skyrme Forces, Hartree-Fock (HF), Random Phase Approximation (RPA), Higher Modes Excited State, Skyrme Energy Density.
PACS: 14.20.Dh, 21.10._k, 21.10.Dr, 21.10.Ft,21.10.Pc,21.60.Cs, 21.60.Jz

INTRODUCTION

The structure of the atomic nucleus is dictated by the interactions of its constituents. Understanding the behavior of multi-degree-of-freedom systems in terms of the fundamental interactions between their constituent components is one of the most difficult challenges in theoretical physics. The theoretical models need to be greatly simplified to find a solution to the problem of many-body in non-relativistic quantum mechanics, which governs self-bound composite systems [1]. When it comes to explaining the structure and dynamical features of nuclei, this is precisely the case [2-4]. A nuclear multi-body issue, which occurs in many disciplines of physics, is notoriously difficult to answer precisely. There are a number of approximate techniques for dealing with such systems. The independent particle approximation is used in the Simple Shell Model (SM), which ignores all correlation effects. The nuclear SM is one of the most important tools for understanding the structure of atomic nuclei and their radioactive decay stability. It is, like the atomic SM, is a microscopic approach that calculates the interaction of individual nucleons with a mean-field potential created by each of the system's constituent nucleons [5]. The nuclear shell model is based on the premise that each nucleon (proton or neutron) travels in the average field independently to the first order. RPA based on Hartree-Fock (HF) has been particularly successful in describing collective motion phenomena in nuclei at the microscopic level [6]. The HF and RPA nuclear structure approaches are widely regarded as highly successful in designing the ground states and excitations of spherical nuclei with effective interactions that are density-dependent [7]. The categorization of excitation modes is contingent upon the process by which a nucleus is excited [8].

In the present, the static and dynamic nuclear properties of some closed-shell nuclei, such as ^{58}Ni, ^{90}Zr, ^{116}Sn, and ^{144}Sm nuclei, were investigated using a basis on Skyrme-type interactions and the self-consistent HF- RPA, SyO+, SyO-, Sk255, SLy4, BSk17, and SLy5. In particular, the charge, neutron, proton, and mass densities associated with root mean square radii (rms) In addition, excitation energy, transition densities, and strength functions for the transition to negative parity states are also included. The estimated result will be compared with the available experimental data. In these nuclei, giant resonance (GR) modes and transition densities were also detected, indicating that the nucleus is moving collectively.

THEORETICAL CONSIDERATION

Hartree-Fock Method

The "self-consistent field" approach was invented by Hartree, which he developed shortly after the formulation of the Schrödinger equations, to approximate the calculation of the wave functions and energy of atoms using the wave function of a single particle, which may be thought of as a combination of many-body wave functions [9]. Using variational principles, the HF equations can be obtained [10]. The variational principle is a method for calculating the wave functions and bound-state energies of a time-independent Hamiltonian [11]. Calculations for closed-shell nuclei were performed using the density-dependent nucleon-nucleon interaction of Skyrme [12]. Which of the following is regarded as a Slater determinant for the single-particle state:

$$\varphi_\beta(x_1,x_2...,x_A)=\frac{1}{\sqrt{A!}}\ \det\left|\varphi_\beta(x_j)\right| \tag{1}$$

where is the set of space $\vec{r}$, σ spin, and q isospin coordinate, A is the number of sets.

† ***Cite as:*** N.M. Kareem, and A.A. Alzubadi, East Eur. J. Phys. **4**, 57 (2022), https://doi.org/10.26565/2312-4334-2022-4-04

The integral of the Hamiltonian density H can be used to expectation the Slater determinant total Hamiltonian's (H) expectation value:

$$\left\langle \varphi \middle| \hat{H} \middle| \varphi \right\rangle = \int \hat{H}(\vec{r})\, d\vec{r} \tag{2}$$

Regarding the HF wave function, the predicted value of the whole Hamiltonian is used to estimate the ground-state energy in the HF approach [11].

$$\begin{aligned} E^0_{HF} &= \left\langle \Phi_{HF} \middle| \hat{H} \middle| \Phi_{HF} \right\rangle = -\frac{\hbar^2}{2m} \sum_{i=1}^{A} \int \phi^*_i(\vec{r}) \nabla^2 \phi_i(\vec{r}) dr \\ &+ \frac{1}{2} \sum_{i \neq j}^{A} \iint \phi_i^*(\vec{r})\, \phi^*_j(\vec{r}')\, V(\vec{r},\vec{r}')\, \phi_i(\vec{r})\, \phi_j(\vec{r}')\, d\vec{r}\, d\vec{r}' \\ &- \frac{1}{2} \sum_{i \neq j}^{A} \iint \phi_i^*(\vec{r})\, \phi_j^*(\vec{r}')\, V(\vec{r},\vec{r}') \phi_i(\vec{r}') \phi_j(r)\, d\vec{r}\, d\vec{r}' \end{aligned} \tag{3}$$

The HF equations are simplified [11].

$$\frac{\hbar^2}{2m} \nabla^2 \Phi_i(\vec{r}) + U_H^{(i)}(\vec{r}) \Phi_i(\vec{r}) - \int U_F^{(i)}(\vec{r},\vec{r}') \Phi_i(\vec{r}')\, d\vec{r}' = \varepsilon_i \Phi_i(\vec{r}) \tag{4}$$

With the addition of a non-local term, it resembles the ordinary one-body Schrödinger equation. The ground state Slater determinant, also known as the solution of the wave function matrix of a single particle, may be used to derive a sequence of one-body densities.

Skyrme-Type Interaction

The Skyrme interaction was developed for nuclear structure computations based on the idea that the energy functional could be rescaled and written as a zero-range expansion. As a result, the HF equations may be inferred easily by exchanging terms with the same mathematical structure as direct terms. Since Brink and Vautherin's pioneering work [13]. The Skyrme interaction is defined as the sum of two and three body components [14]. It is possible to express the interaction between two nucleons with $\mathbf{r_1}$and $\mathbf{r_2}$ spatial coordinates in the standard form [15]:

$$\begin{aligned} \mathrm{V}(\vec{\mathrm{r}}_1, \vec{\mathrm{r}}_2) &= \mathrm{t}_0\left(1 + \mathrm{x}_0 \hat{\mathrm{P}}_\sigma\right)\delta_{12} + \frac{\mathrm{t}_1}{2}\left(1 + \mathrm{x}_1 \hat{\mathrm{P}}_\sigma\right)\left[\delta_{12}\vec{\mathrm{k}}^2 + \delta_{12}\mathrm{k}'^2\right] + \\ &\mathrm{t}_2\left(1 + \mathrm{x}_2 \hat{\mathrm{P}}_\sigma\right)\hat{\mathrm{k}}'\delta_{12}\hat{\mathrm{k}} + \frac{\mathrm{t}_3}{6}\left(1 + \mathrm{x}_3 \hat{\mathrm{P}}_\sigma\right)\rho^\alpha\left(\frac{\vec{r}_1 + \vec{r}_2}{2}\right)\delta_{12} + \\ &\mathrm{i}\mathrm{W}_0\left(\hat{\sigma}_1 + \hat{\sigma}_2\right)\cdot\left[\hat{\mathrm{k}}' \times \delta_{12}\hat{\mathrm{k}}\right] \end{aligned} \tag{5}$$

where, $\delta_{12} = \delta(\vec{r}_1 - \vec{r}_2)$ is the interaction Dirac delta function [16], $\boldsymbol{\sigma}$ are the Pauli spin matrices and $\hat{\mathrm{P}}_\sigma = (1 + \hat{\sigma}_1 . \hat{\sigma}_2)/2$ is the spin exchange operator, while $\hat{k}'$ and $\hat{k}$ are the operators for relative momentum. k' acting on the right and k' acting on the left. They are defined as follows: $\hat{k}' = -\frac{1}{2i}(\vec{\nabla}_1 - \vec{\nabla}_2)$ and $\hat{k} = \frac{1}{2i}(\vec{\nabla}_1 - \vec{\nabla}_2)$.

The free parameters t_1, t_0, t_3, t_2, x_0, x_1, x_2, x_3, and W_0, to produce the experimental data obtained from a limited number of nuclei, including binding energies as well as rms radii, are combined with the theory of nuclear matter properties.

Skyrme Energy Density

The Skyrme energy density functional, which is a function of various densities, can be calculated using the conventional Skyrme force [15]. The integral of the Hamiltonian density H can be used to calculate the probability value for the total Hamiltonian (H) of the Slater determinant:

$$\mathrm{E}[\rho] = \langle \psi | \mathrm{T} + \mathrm{V}_{\mathrm{Skyrme}} | \psi \rangle = \int \mathrm{d}^3\mathrm{r}\, \mathrm{E}(\mathrm{r}). \tag{6}$$

The Hamiltonian operator can be expressed as a sum of terms representing various aspects of the force [15]:

$$\hat{H} = \hat{H}_{kin} + \hat{H}_0 + \hat{H}_3 + \hat{H}_{eff} + \hat{H}_{fin} + \hat{H}_{so} + \hat{H}_{sg} + \hat{H}_{Coul} \tag{7}$$

Skyrme-Hartree-Fock Equations

It's difficult to represent the system's energy as a function of the standard density matrix using the Skyrme interaction because of the dependence on *J*. In this situation, the energy must be adjusted with single-particle wave functions, with the additional stipulation that the φ_k is normalized [17].

$$\delta\left[E-\sum_{i}\varepsilon i\int d^3r\left|\phi i(r)\right|^2\right]=0\,, \tag{8}$$

$$\delta E=\sum_{q}\int d^3r\left[\frac{\hbar^2}{2m_q^{*}(r)}\delta\tau_q(r)+\mathrm{U_q}\left(\mathrm{r}\right)\delta\rho_q(r)+w_q(r).\delta J_q(r)\right], \tag{9}$$

where the coefficients of the variation are,

$$\frac{\hbar^2}{2m_q^{*}}=\frac{\delta E}{\delta\rho_q}=\frac{\hbar^2}{2m_q}+\frac{1}{8}\left[t_1(2+x_1)+t_2(2+x_2)\right]\rho+\frac{1}{8}\left[t_2(2x_2+1)-t_1(2x_1+1)\right]\rho_q\ , \tag{10}$$

$$\begin{aligned}U_q=\frac{\delta E}{\delta\rho_q}&=\frac{1}{2}\mathrm{t_0}\ \left[(2+x_0)-\rho(2x_0+1)\right]+\frac{1}{24}\mathrm{t_3}\alpha\rho^{\alpha\text{-}1}\left[\ (2+x_3)\rho^2-(2x_3+1)({\rho_p}^2+{\rho_n}^2)\right]\\&+\frac{1}{12}\ \mathrm{t_3}\rho^{\alpha}\left[\ (2+x_3)\rho-(2x_3+1)\rho_q\right]+\frac{1}{8}\left[t_1(2+x_1)+t_2(2+x_2)\right]\tau+\frac{1}{8}\left[t_2(2x_2+1)-t_1(2x_1+1)\right]\tau_{\mathrm{q}}\\&-\frac{1}{16}\left[3t_1(2+x_1)-t_2(2+x_2)\right]\nabla^2\rho+\frac{1}{16}\ \left[3t_1(2x_1+1)+t_2(2x_2+1)\right]\nabla^2\rho_q-\frac{1}{2}\mathrm{W_0}\left[\ \nabla.J+\nabla.J_q\right]+\delta_1 qV_C\end{aligned}\ , \tag{11}$$

$$W_q=\frac{\delta E}{\delta J_q}=\frac{1}{2}\ \mathrm{W_0}\left[\nabla\rho+\nabla\rho_q\right]-\frac{1}{8}(\mathrm{t_1x_1+t_2x_2})\mathrm{J}+\frac{1}{8}(\mathrm{t_1\text{-}t_2})\mathrm{J_q}\,, \tag{12}$$

assuming a spherical closed-shell nucleus. As a result, the SHF radial equations can be deduced [18] which give can be deduced.

$$\begin{aligned}&\frac{\hbar^2}{2m^{*}{}_q(r)}\left[\ -u'\,'{}_q(r)+\frac{l(l+1)}{r^2}\mathrm{u}_\alpha(\mathrm{r})\ \right]-\frac{d}{dr}\left(\ \frac{\hbar^2}{2m^{*}{}_q(r)}\right)u_\alpha'(r)\\&+\left\{U_q(r)+\frac{1}{r}\ \frac{d}{dr}\left(\ \frac{\hbar 2}{2m^{*}{}_q(r)}\ \right)+\left(\ j(j+1)-l(l+1)-\frac{3}{4}\ \right)\frac{W_q(r)}{r}\ \right\}u_\alpha(r)=\varepsilon_\alpha u_\alpha(r)\end{aligned}\ . \tag{13}$$

The Random Phase Approximation

RPA is commonly regarded as a suitable method for studying nuclear structure since it provides an effective formalism for describing numerous giant resonances or excitations caused by low-lying particle holes, which are examples of nuclear excitations [19]. This theory can be used to describe the properties of low-energy excited states [20].
The straightforward HF Slater-determinant of the Schrödinger equation for this situation is [21].

$$H^{\hat{}}\left|v\right\rangle=E_v\left|v\right\rangle, \tag{14}$$

The so-called creation operators $Q_{\mathrm{v}}^{\dagger}$ can be employed to express the eigenvectors $\left|v\right\rangle$.

$$\left|v\right\rangle=Q_{\mathrm{v}}^{\dagger}\left|0\right\rangle, \tag{15}$$

where $\left|0\right\rangle$, the ground state, is also known as the vacuum.

In the RPA, we can generate and annihilate *p-h* pairs; the real ground state is not merely the HF vacuum [21].

$$Q_v^{\dagger}(JM)=\sum_{ab}X_{ab}{}^{v}A_{ab}{}^{\dagger}(JM)-Y_{ab}\tilde{A}_{ab}(JM)\,. \tag{16}$$

Hermitian conjugation yields the following annihilation operator:

$$Q_v=\sum_{ab}\left[\ X_{ab}{}^{v*}A_{ab}(JM)-Y_{ab}{}^{v*}\tilde{A}_{ab}{}^{\dagger}(JM)\right]. \tag{17}$$

The state's excitation energy $\left|v\right\rangle$ and the correlation matrix $\hbar w_v=E_v-E_0$ are combined into one matrix equation [21].

$$\begin{pmatrix} A & B \\ -B^* & -A^* \end{pmatrix} \begin{pmatrix} X_{(v)} \\ Y_{(v)} \end{pmatrix} = \hbar w_v \begin{pmatrix} X_{(v)} \\ Y_{(v)} \end{pmatrix}. \quad (18)$$

If the size of the *p-h* configuration space is *N*, the matrices elements. The sub matrices *B*and *A* are formed from the particle-hole configurations, where matrix *A* is Hermitian and the correlation matrix *B* is symmetric [22].
With the use of a multipole, transition density characterizes the connection between each excited state and the ground state. A transition is a generated amplitude for the operator. It is possible to compute its transition density's radial component. It has the definition below [23]:

$$\delta\rho_v(\vec{r}) = \langle v|\hat{\rho}(\vec{r})|0\rangle = \delta\rho_v(r)\,\psi^*_{(JM)}(\hat{r}). \quad (19)$$

Below is the description of the density of state radial transition [23].

$$\delta\rho_v = \frac{1}{\sqrt{2J+1}} \sum_{mi} \left[X^{(v)}_{mi} + Y^{(v)}_{mi} \right] \langle m \| Y_J \| i \rangle \frac{u_m(r)\,u_i(r)}{r^2}\,, \quad (20)$$

Excitation characteristics such as volume or surface type can be revealed through transition densities. The transition density for neutrons and protons is given as it can be either an isoscalar (IS) (T = 0) or an isovector (IV) (T = 1) [23]:

$$\delta\rho_v^{IS}(r) = \delta\rho_{vn}(r) + \delta\rho_{vp}(r);\ \Delta T = 0\,, \quad (21)$$

$$\delta\rho_v^{IV}(r) = \delta\rho_{vn}(r) - \delta\rho_{vp}(r);\ \Delta T = 1\,. \quad (22)$$

In general, spherical harmonics related sum rule features can be enlarged in IS and IV external fields (F). It is possible to compute it using [23]. It can be calculated from:

$$\hat{\mathrm{F}}_{\mathrm{J}}^{(\mathrm{IV})} = \sum_{i=1}^{A} f_J(\vec{r}_i) Y_{JM}(\vec{r}_i)(\tau_z), \quad (23)$$

$$\hat{\mathrm{F}}_{\mathrm{J}}^{(\mathrm{IS})} = \sum_{i=1}^{A} f_J(\vec{r}_i) Y_{JM}(\vec{r}_i)\,. \quad (24)$$

The IS and IV giant resonances' strength function distributions S(E) have been discovered to be extremely sensitive to nuclear matter's physical characteristics. The strength function of low-lying energy could be calculated by using the following:

$$S(E) = \sum_v \left| \langle v \| \hat{F}_J \| 0 \rangle \right|^2 \delta(E - E_v)\,. \quad (25)$$

When the sum rule characteristics of generic IS and IV external fields are connected [23]. We can calculate the energy moments by integral the strength function, S(E).

$$m_k = \int_{E_1}^{E_2} E^k S(E) dE\,. \quad (26)$$

where E1 and E2 are the excitation energy limits. The energy moments can be calculated using the formula integrating the strength function S(E). These densities can be used for calculating the rms radius of neutrons, protons, charge, and mass distributions [13], [24]:

$$r_q = \left\langle r_q^{\,2} \right\rangle^{\frac{1}{2}} = \left[\frac{\int r^2 \rho_q(r) \mathrm{d}r}{\int \rho_q(r) \mathrm{d}r} \right]^{\frac{1}{2}}. \quad (27)$$

The proton radius is used to determine the charge radius [22].

$$\left\langle r_{ch}^{\,2} \right\rangle = \left\langle r_p^{\,2} \right\rangle + \left\langle r \right\rangle_p^{\,2}, \quad (28)$$

where the proton's rms charge radius is 0.8 fm. The neutron skin thickness **t** is calculated using the difference in rms radii between the proton and the neutron. This difference provides information on the structure of nuclei [13].

$$\Delta r_{np} = \left\langle r^2 \right\rangle_n^{\frac{1}{2}} - \left\langle r^2 \right\rangle_p^{\frac{1}{2}}. \quad (29)$$

RESULTS AND DISCUSSION

The Nuclear Ground State Properties

The ground state nuclear properties of an HF, such as the charge density distribution rms, and the binding energies per nucleon and neutron skin thickness, were calculated and compared using several Skyrme parameterizations: Sk255,

BSk17, SyO+, SyO-, SLy4 and SLy5. These parameterizationsare described in tabulated 1. Tables (2–5) show the calculated static nucleon properties for the closed-shell nuclei chosen using these parameterizations in conjunction with experimental data from Refs. [25,26]. In the microscopic model, the radius values have risen from 3.7 fm (for ^{58}Ni) to 4.9 fm (for ^{144}Sm). And the binding energies per nucleon are in the range(8.68.26) MeV. This means that the binding energy per particle is nearly 8 MeV. From the tabulated results, it is clear that charge rms radius values in BSk17 parameterization are the closest to experimental data for ^{58}Ni and ^{116}Sn, followed by the results of SyO+ for ^{90}Zr and SLy5 for ^{144}Sm.

The nuclear charge densities provide a description of a nucleus' interior structure. Fig. 1 depicts the estimated HF radial charge density distribution for a single particle for ^{58}Ni, ^{90}Zr, ^{116}Sn, and ^{144}Sm, respectively. A comparison was made with the available experimental data ^{58}Ni, ^{90}Zr, ^{116}Sn, and ^{144}Sm, respectively. A comparison was made with the experimental data [27,28] except for ^{116}Sn, for which no available experimental data exists. The ^{58}Ni results are in complete good agreement with experimental data using SLy5, SLy4, BSk17, SyO-and SyO+ parameterizations. However, the Sk255 results are comparable to experimental evidence but do not fit within the nucleus. For ^{90}Zr, the SLy4, BSk17, SLy5, and Sk255 parameterizations coincide quite well. However, the results for SyO+ and SyO- are close to the experimental data but don't fit inside the nucleus. For ^{116}Sn Sk255, BSk17, SyO+, SLy5, SLy4, and SyO-parameterizations, although the findings are comparable to experimental data, they do not fit inside the nucleus. Consideration must also be given to the fact that nucleons possess intrinsic electromagnetic structure. Therefore, the proton, neutron, and mass density profiles must be computed. The profile of every nuclear density type of each of the chosen nuclei is shown in Fig. 2. Examining these curves demonstrates that the nuclear charge distributiondensity is depends on the rms radius, which rises as the number of protons in each nucleus increases. As the nucleus radius rose for ^{144}Sm, the density distributions for mass, charge, proton, and neutron increased. While in ^{58}Ni, ^{90}Zr, and ^{116}Sn, the charge density distributions gradually declined as the nucleus' radii shrank. From Tables (2–5), it is evident that the energy per nucleon for all nuclei match with experimental data, particularly when the SLy5 and SLy4 parameterizations are used. In Figs. (3, 4), the theoretical rms charge radii and the binding energies per nucleon for closed-shell nuclei are compared with experimental data from Refs. [25], [26]. Very good agreement with experiments is seen, especially when Skyrme parameterization is used.

Table 1. The Skyrme parameterizations used in the present work.

Parameters	BSk17 [29]	Sk255 [30]	SyO+[31]	SyO-[31]	SLy4 [15]	SLy5 [15]
t_0 (MeV fm^3)	-1837.33	-1689.35	-2099.419	-2103.653	-2488.91	-2484.88
t_1 (MeV fm^5)	389.102	389.3	301.531	303.352	486.82	483.13
t_2 (MeV fm^5)	-3.1742	-126.07	154.781	791.674	-546.390	-549.40
t_3 (MeV fm$^{3+3\alpha}$)	11523.8	10989.6	13526.464	13553.252	13777.0	13763.0
x_0	0.411377	-0.1461	-0.029503	-0.210701	0.834	0.778
x_1	-0.832102	0.116	-1.325732	-2.810752	-0.344	-0.328
x_2	49.4875	0.0012	-2.323439	-1.461595	-1.0	-1.0
x_3	0.654962	-0.7449	-0.147404	-0.429881	1.354	1.267
w_0 (MeV fm^5)	145.885	95.39	287.79	353.156	123.0	126.0
$w`_0$ (MeV fm^5)	145.885	95.39	-165.7776	-397.498	123.0	126.0
A	0.3	0.3563	0.25	0.25	0.1666666	0.1666666

Table 2. The calculated binding energy per nucleon, neutron, proton, mass, charge radii, and also the neutron skin thickness (tn), for ^{58}Ni by using different Skyrme parameterizations.

Force	Rn(fm)	Rp(fm)	Rm(fm)	Rc(fm) Theo.	t_n(fm)	Rc(fm) Exp. [25]	B/A(MeV) Theo.	B/A(MeV) Exp. [26]
BSk17	4.2669	4.2017	8.4686	4.2764	0.0652	4.2694	-8.9177121	-8.710
Sk255	4.3104	4.2024	8.5128	4.2771	0. 108		-8.9674868	
SyO+	4.2785	4.1674	8.4459	4.2427	0.1111		-8.8412684	
SyO-	4.3010	4.1651	8.4661	4.2405	0.1359		-8.8117009	
SLy5	4.2871	4.2211	8.5082	4.2955	0.066		-8.7051038	
SLy4	4.2875	4.2251	8.5126	4.2994	0.0624		-8.7320496	

Table 3. The calculated binding energy per nucleon, neutron, proton, mass, charge radii, and.also the neutron skin thickness (tn), for ^{90}Zr by using different Skyrme parameterizations.

Force	Rn(fm)	Rp(fm)	Rm(fm)	Rc(fm) Theo.	t_n(fm)	Rc(fm) Exp. [25]	B/A(MeV) Theo.	B/A(MeV) Exp. [26]
BSk17	3.6890	3.6923	7.3813	3.7771	-0.0033	3.7757	-8.9121212	-8.732
Sk255	3.7272	3.7172	7.4444	3.8015	0.01		-8.8322377	
SyO+	3.6812	3.6730	7.3542	3.7583	-0.0082		-8.8506103	
SyO-	3.6780	3.6713	7.3493	3.7565	0.0067		-8.8691517	
SLy5	3.7097	3.7114	7.4211	3.7957	-0.0017		-8.6936665	
SLy4	3.7128	3.7159	7.4287	3.8001	-0.0031		-8.7065109	

Table 4. The calculated binding energy per nucleon, neutron, proton, mass, charge radii, and. also the neutron skin thickness (tn), for ^{116}Sn by using different Skyrme parameterizations.

Force	Rn(fm)	Rp(fm)	Rm(fm)	Rc(fm) Theo.	t_n(fm)	Rc(fm) Exp. [25]	B/A(MeV) Theo.	B/A(MeV) Exp. [26]
BSk17	4.6403	4.5458	9. 1861	4.6150	0.0945	4.6250	-8.6701555	-8.523
Sk255	4.6933	4.5440	9.2373	4.6132	0.1493		-8.7335998	
SyO+	4.6364	4.5294	9.1658	4.5988	0.107		-8.6147510	
SyO-	4.6480	4.5364	9.1844	4.6057	0.1116		-8.6209021	
SLy5	4.6593	4.5620	9.2213	4.6310	0.0673		-8.4741056	
SLy4	4.6636	4.5668	9.2304	4.6356	0.0968		-8.4858585	

Table 5. The calculated binding energy per nucleon, neutron, proton, mass, charge radii, and. also the neutron skin thickness (tn), for ^{144}Sm by using different Skyrme parameterizations.

Force	Rn(fm)	Rp(fm)	Rm(fm)	Rc(fm) Theo.	t_n(fm)	Rc(fm) Exp. [25]	B/A(MeV) Theo.	B/A(MeV) Exp. [26]
BSk17	4.9436	4.8697	9.8133	4.9343	0.0739	4.9524	-8.4640657	-8.304
Sk255	5.0028	4.8717	9. 8745	4.9363	0.1311		-8.5106563	
SyO+	4.9585	4.8443	9.8028	4.9092	0.1142		-8.3523560	
SyO-	4.9792	4.8463	9.8255	4.9112	0.1329		-8.3412634	
SLy5	4.9620	4.8853	9.8473	4.9497	0.0767		-8.2672154	
SLy4	4.9659	4.8920	9.8579	4.9564	0.0739		-8.2278044	

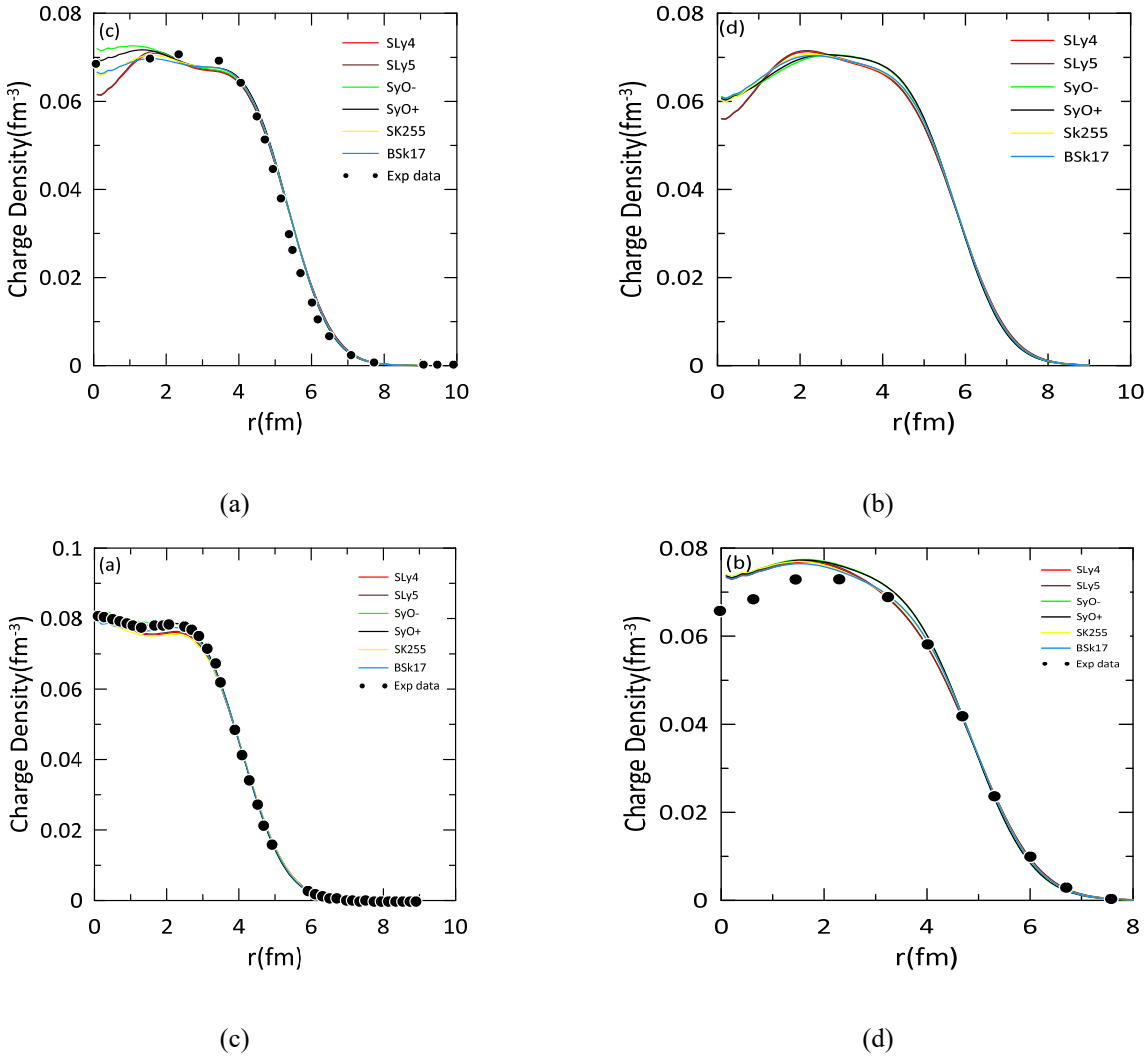

Figure 1. The calculated charge density distribution profiles of the magic nucleus (a) ^{58}Ni, (b) ^{90}Zr, (c) ^{116}Sn, and (d) ^{144}Sm in comparison with known experimental results (closed dots) collected from Refs. (^{58}Ni and^{90}Zr) [27], (^{116}Sn) [28].

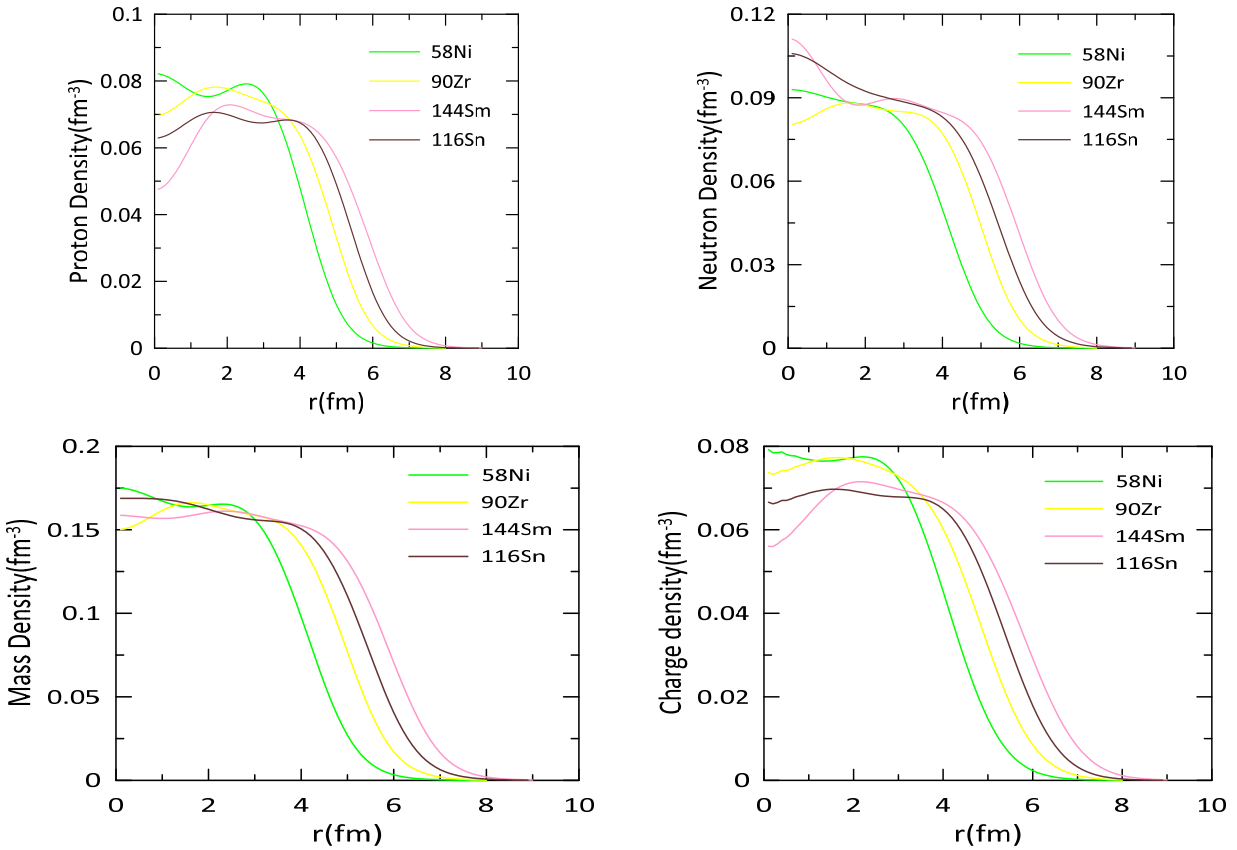

Figure 2. Calculated of proton, mass, neutron, and charge density distributions for closed-shell nuclei ^{58}Ni, ^{90}Zr, ^{116}Sn and ^{144}Sm using SCRPA

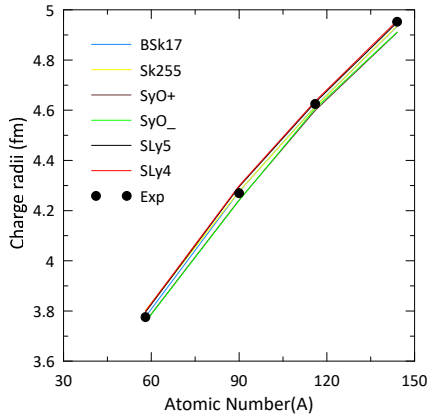

Figure 3. The Nuclear root-mean-square(rms) charge radii for closed shell nuclei as a function of nucleon number A, compared with data from experimental Ref. [25]

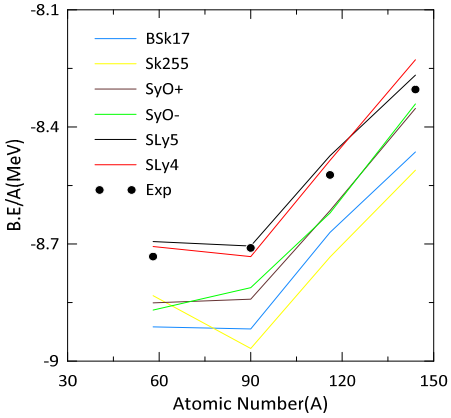

Figure 4. Nuclear B.E/A for closed shell nuclei as a function of nucleon number A, compared with data from experimental Ref. [26]

The Excited States Properties

RPA calculations were widely utilized to describe the transition densities of the proton and neutron as well as GRs modes. This technique classifies collective resonances of various multipolarities, like the giant dipole photon absorption cross-section multipole at rank 2, referred to as isoscalar giant dipole resonance (ISGDR), rank 3 is giant octupole resonance (GOR), rank 5 is giant triacontadipole resonance (GTR), and rank 7 is giant octacosahectapole resonance (GOCR). In addition, the relation between the IV and IS strength functions and also the excitation energy functions has been defined, as have multipole excitations characterized by p-h pairings in which the particles and hole states are slightly below and above the Fermi surface. For optimum results, SLy5 and SLy4 parameterizations were chosen for this purpose based on the best binding energy estimates compared with experimental data [26].

Transition density calculation. For collective electric excitations, the transition density is useful for the low-lying excited states for nuclei ^{58}Ni, ^{90}Zr, ^{116}Sn and ^{144}Sm, The radial transition densities of protons and neutrons for the RPA state are shown in Figs. (5–12).

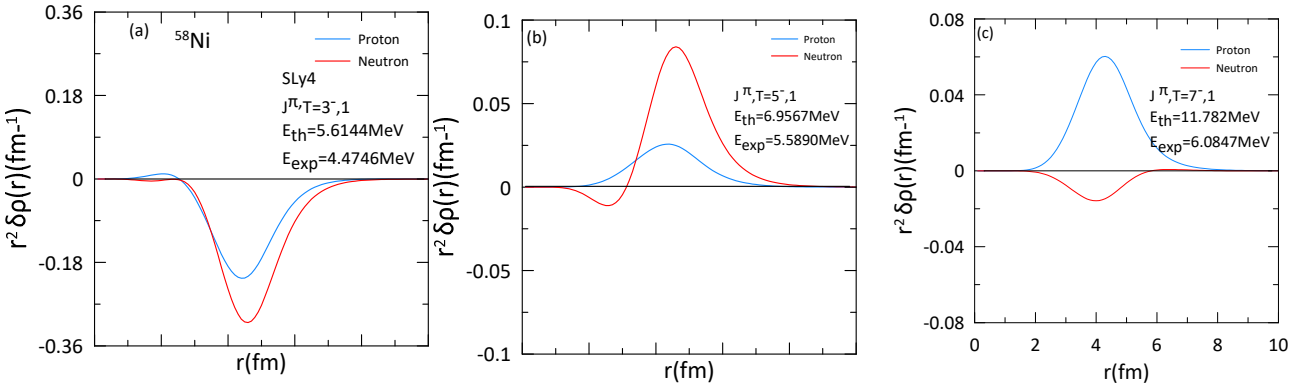

Figure 5. The radial transition densities of protons and neutrons for the negative parity state are shown for ^{58}Ni (a) 3$^-$, (b) 5$^-$ and (c) 7$^-$ using RPA with SLy4 Skyrme parameterization. The energy of excitation was compared with experimental data taken from Ref. [33]

Compared to the existing experimental data, the estimated excitation energy of the negative parity excited states is qualitatively consistent with the results of the experiments (^{90}Zr has state 3$^-$(2.747875MeV), ^{116}Sn has states 3$^-$(2.66159MeV) and 7$^-$(2.90885MeV), and ^{144}Sm has state 5$^-$(2.82517MeV)). There is a small difference between theoretical values and experimental data for (^{58}Ni with states 3$^-$(4.971MeV) and 5-(5.5890MeV)), (^{90}Zr with states 5$^-$(2.319000MeV) and 7$^-$(4.037507MeV)), (^{116}Sn with state 1$^-$(6.020MeV)), and (^{144}Sm with state 7$^-$(3.12407MeV)) and a significant difference for (^{58}Ni with state 7$^-$(6.00847MeV)) and (^{90}Zr with state 1$^-$(6.020 MeV)). The associated transition densities effectively represent density oscillations around the ground state configuration. It is a crucial characteristic that sheds light on the nature of nuclear excitations in excited states, which determine protons and neutrons responses to external disturbance to obtain a simple estimation of the collectivity shown by the various dipole responses. It is shown that protons and neutrons can vibrate either in the skin mode's IS phase, where protons oscillate against neutrons, or in phase IV, which is the opposite (pn mode). Furthermore, the IV characterization is crucial for describing the motion of the neutron and proton within the nucleus, as it appears the peaks for proton and neutron transition densities appear to be positive for both protons and neutrons. The quantum numbers identifying these p-h pairs' SP states are identical. The electric multipole excitations (Jπ = 1–, 3–, 5–, 7–) emphasize this section of the current work. GR states are classified using the spin S, isospin T transmitted and total angular momentum J, as a result of nuclear ground state excitation. The scope of this study was confined to electric IS resonance with S = 0 and T = 0.Electric IV resonance takes place when S = 1 and T = 1.

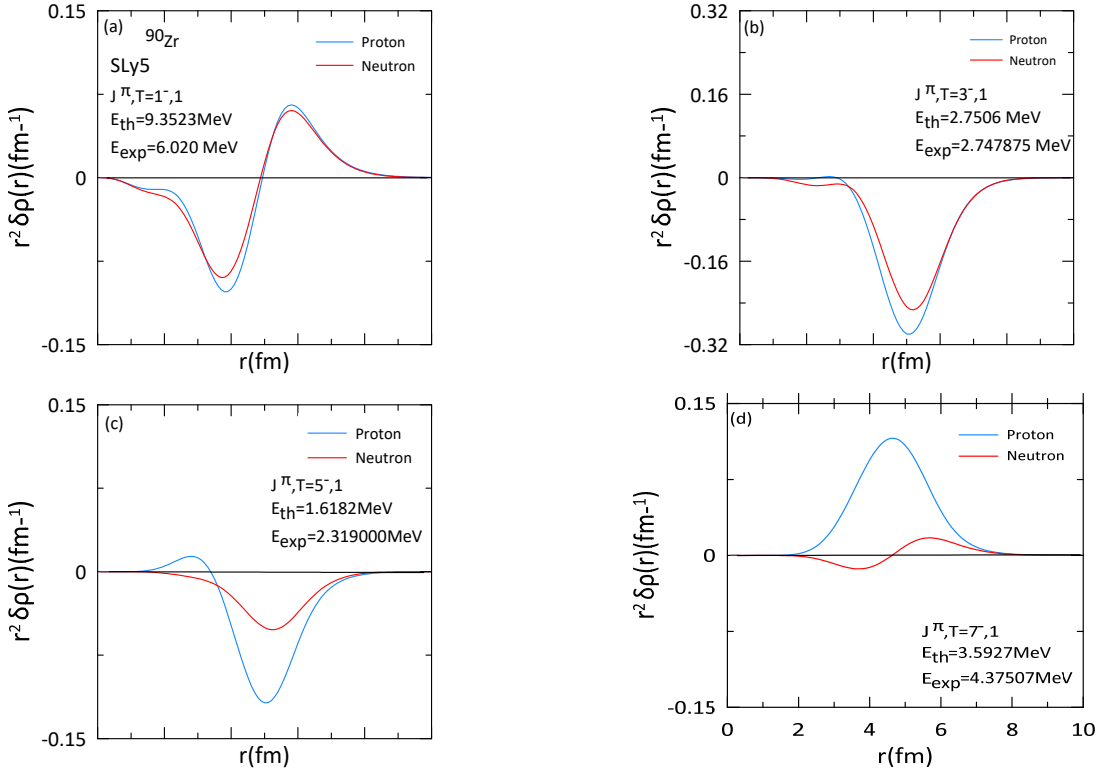

Figure 6. Same as **Fig. 5** but using RPA with SLy5 Skyrme parameterization. For ^{90}Zr nucleus (a) 1, (b) 3$^-$, (c) 5$^-$ and (d) 7$^-$

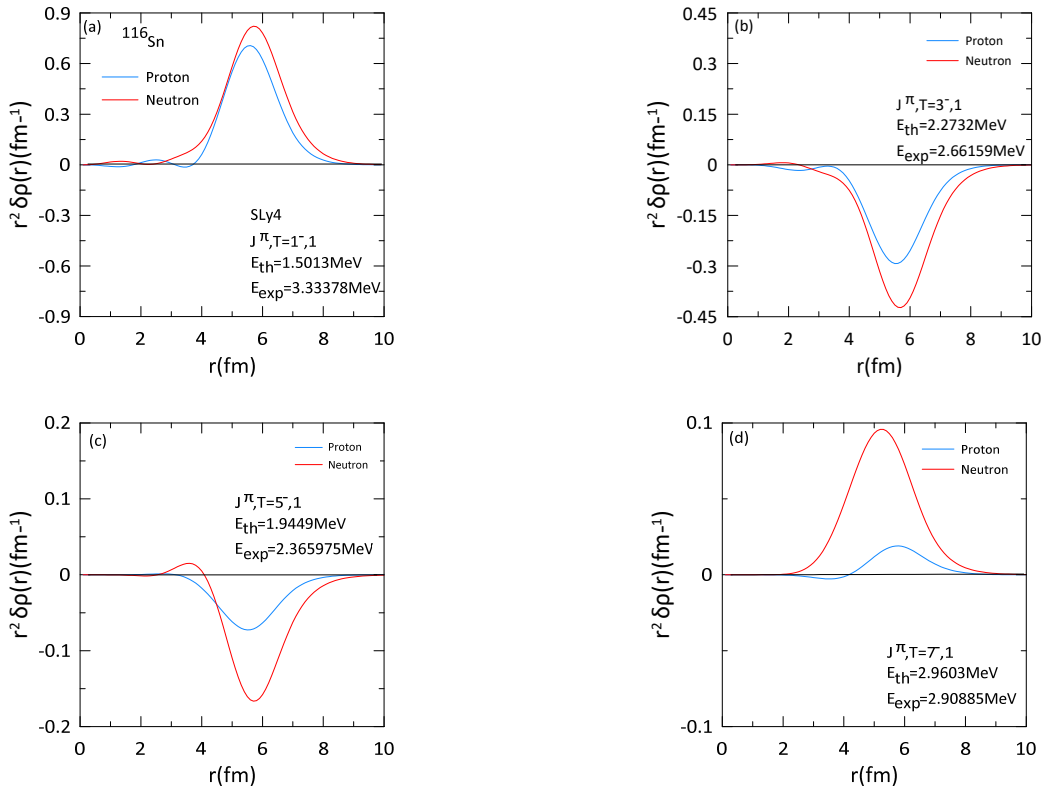

Figure 7. The radial transition densities of protons and neutrons for the negative parity state are shown for ^{116}Sn (a) 3^-, (b) 5^- and (c) 7^- using RPA with SLy4 Skyrme parameterization. The energy of excitation was compared to the experimental results obtained from Ref. [33]

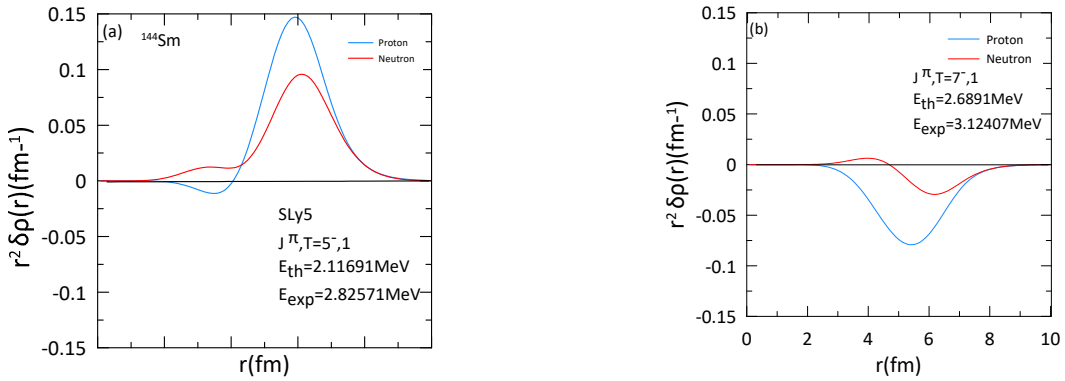

Figure8. Same as **Fig. 7** but using RPA with SLy5 Skyrme parameterization. For ^{144}Sm nucleus (a) 5^-, and (b) 7^-

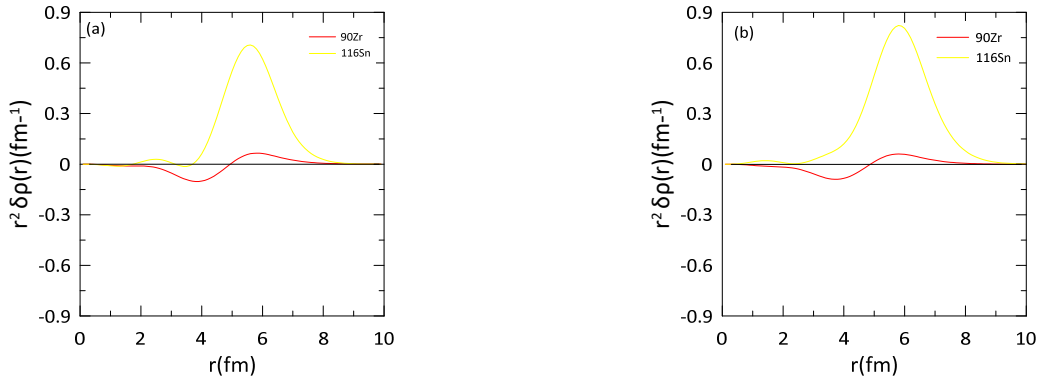

Figure 9. The proton (a) and neutron (b) transition densities for the transition to the 1^- statein ^{90}Zr and^{116}Sn nuclei using SLy5 and SLy4 Skyrme parameterizations

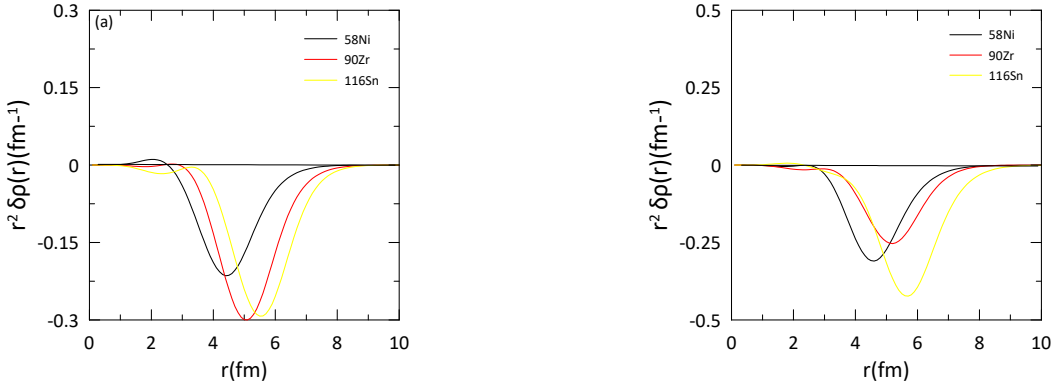

Figure 10. The proton (a) and neutron (b) transition densities for the transition to the 3⁻ state in ^{58}Ni, ^{90}Zr and^{116}Sn nuclei using SLy5 and SLy4 Skyrme parameterizations

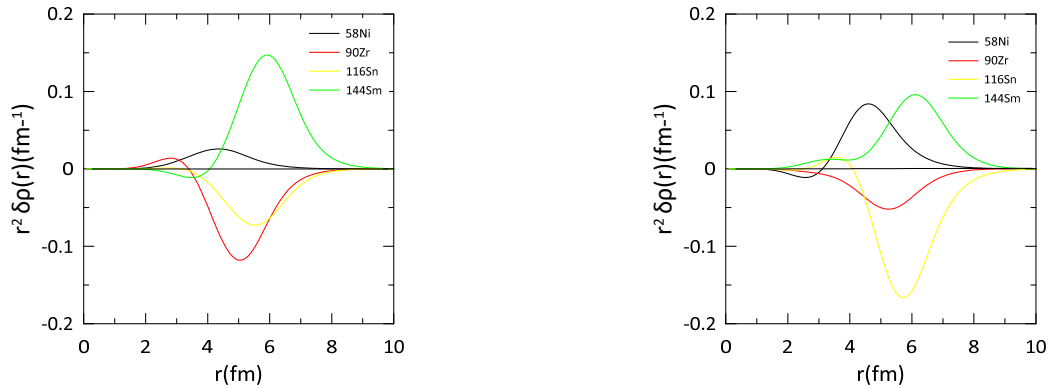

Figure 11. The proton (a) and neutron (b) transition densities for the transition to the 5⁻ state in ^{58}Ni, ^{90}Zr ,^{116}Sn and ^{144}Sm nuclei using SLy5 and SLy4 Skyrme parameterizations.

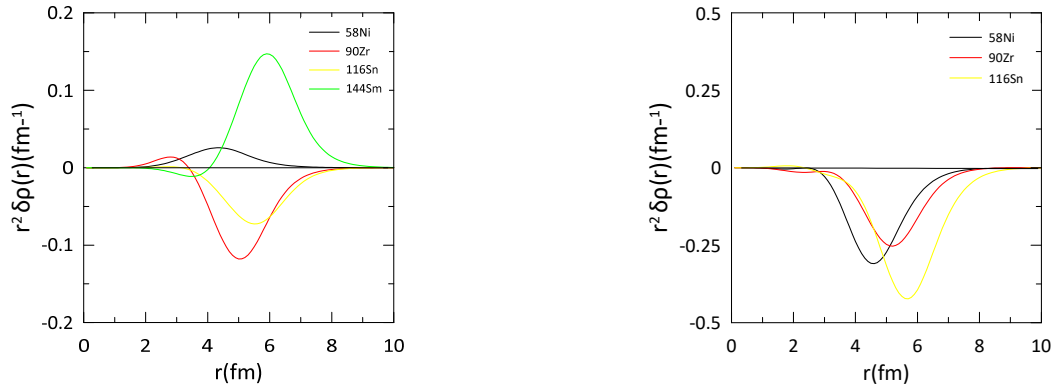

Figure 12: The proton (a) and neutron (b) transition densities for the transition to the 7⁻ state in ^{58}Ni, ^{90}Zr ,^{116}Snand ^{144}Sm nuclei using SLy5 and SLy4 Skyrme parameterizations

Giant Resonance Modes. The most visible manifestation of nucleon collective motion is GRs. Figs. 13-16 show the strength functions for the excitation to the negative parity states in ^{58}Ni, ^{90}Zr, ^{116}Sn, and ^{144}Sm nuclei. The ISGDR is significantly fragmented compared to ISGTR, ISGOR, and ISGOCR, which appear to be less fragmented. This was reflected in IVGTR, IVGOR, IVGDR, and IVGOCR. This indicates that the collective strength of high multipolarity GRs is distributed, and the quantity of collective strength falls as the multipolarity ∇J of the GRs [32]. It is important to note that the IS mode is produced when the neutrons and protons vibrate in phase, while the IV mode is produced when they vibrate in the opposite phase. The higher modes of strength functions for higher modes emerge clearly using RPA approach calculations, which explored upper-level excitation and yielded the collective nuclear motion of nucleons, energy, spin, and parity, all properties of exciting levels. This emphasized the significance of calculating GR strength functions using completely self-consistent HF-based RPA. Collective motion was believed to be a common characteristic of quantum many-body systems. It is believed that the distribution of transition strengths of a low external field that excites the nucleus exhibits resonance peaks that correspond to the elementary vibrational collective modes.

Tables (6-9) summarize the overall calculated results of the EWSR m1 and RPA m1 using SLy5 parameterizations. The total EWSR of strengths is growing compared to those computed using RPA. Therefore, m1 includes those from p-h strengths. The D.C (represents the double commutator which gives EWSR). The deviations of m1 (RPA) from m1 (EWSR) from R values are minor for all collective modes, indicating high precision for self-consistent HF-RPA calculations. It is also worth mentioning that it is the most widely used. The GDR is a well-studied GR wherein protons vibrate collectively against neutrons. This, in the end, shows how strongly neutrons and protons interact inside the nucleus, which is a key part of nuclear interaction.

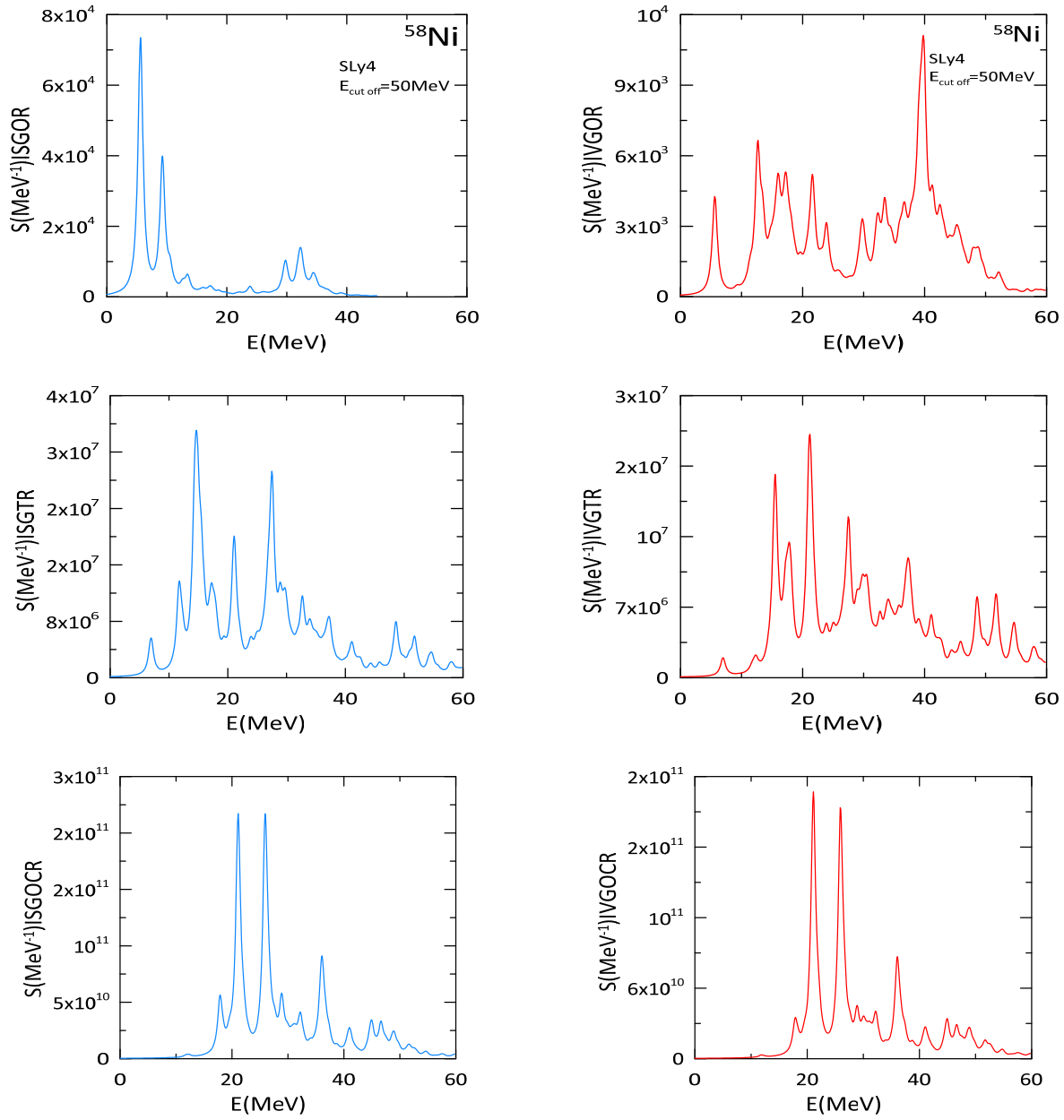

Figure 13. IS (left panel) as well as IV (right panel) HF-based RPA strength function for the octopole (E3),triacontadipole (E5), and octacosahectapole (E7) in ^{58}Ni, using the SLy4 Skyrme interaction

Table 6. The realisation of the EWSR (m1) for the IS and IV within the RPA using multipoles J for 58Ni.Using the SLy5 parametrization with the summing from 0 to E_{max}= 60 MeV.MeVfm^{2J} are the units. R = m1(RPA) / m1 (D.C.)

J^{π}	T	m1 (RPA)	m1(D.C)	R
3^-	0	3.84191×10^{6}	3.64699×10^{6}	1.05344
	1	4.17831×10^{6}	3.98378×10^{6}	1.04883
5^-	0	1.06005×10^{11}	1.01450×10^{11}	1.04489
	1	1.08982×10^{11}	1.05378×10^{11}	1.03420
7^-	0	4.71703×10^{13}	4.30197×10^{13}	1.09648
	1	4.74086×10^{13}	1.37570×10^{17}	3.44614×10^{-4}

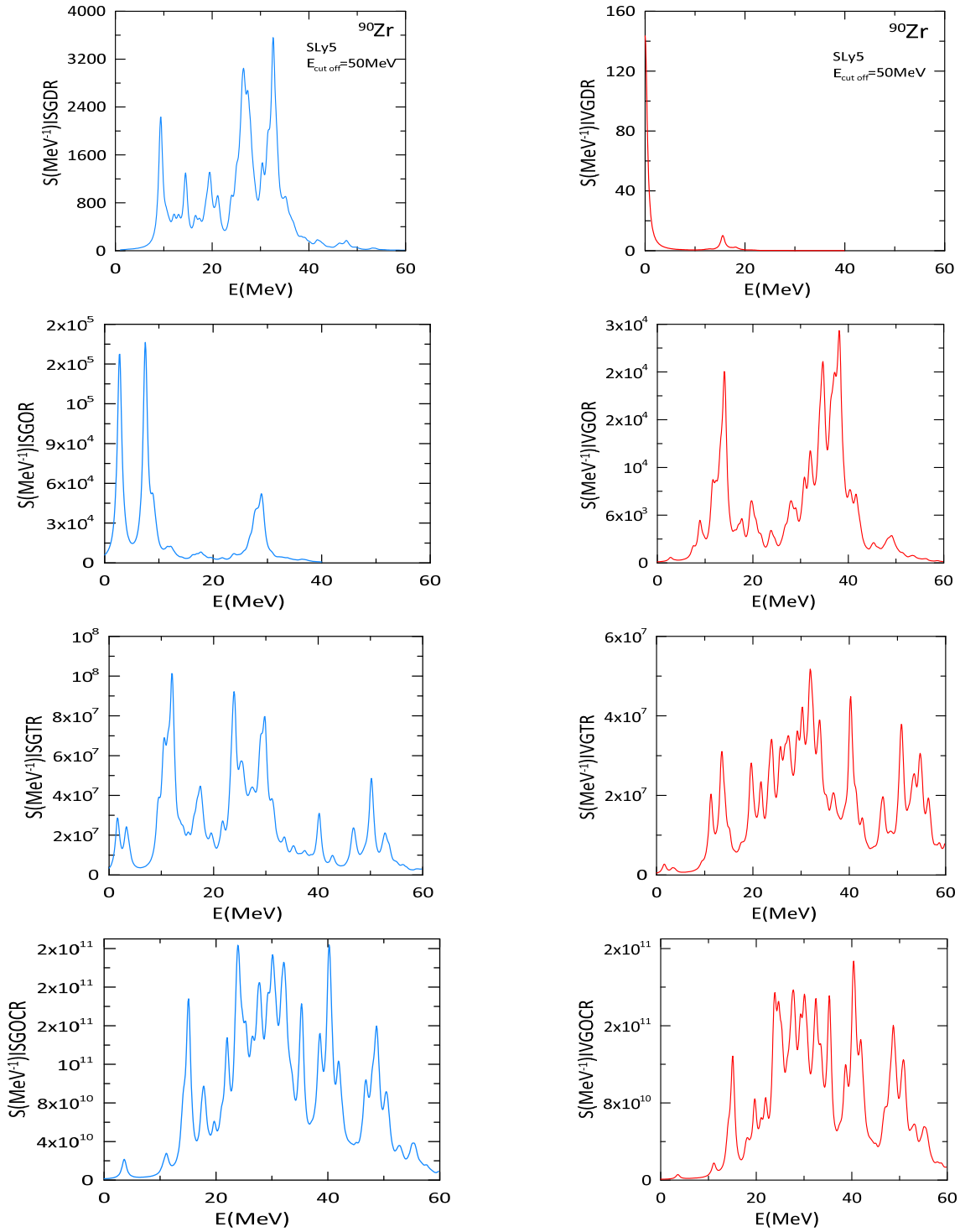

Figure 14. IS (left panel) as well as IV (right panel) HF-based RPA strength function for the dipole photo absorption cross section (E1), octopole (E3), triacontadipole (E5), and octacosahectapole (E7)

Table 7. The same as Table 6, for ^{90}Zr. The results are obtained by using the SLy4 parameterization.

J^{π}	T	m1 (RPA)	m1(D.C)	R
1^-	0	9.02386×10^{5}	9.14815×10^{5}	0.98641
	1	3.84977×10^{2}	3.88898×10^{2}	0.98991
3^-	0	9.41224×10^{6}	9.51103×10^{6}	0.98961
	1	1.03355×10^{7}	1.04769×10^{7}	0.98650
5^-	0	3.77037×10^{10}	3.90294×10^{10}	0.96603
	1	3.92052×10^{10}	4.09882×10^{10}	0.95649
7^-	0	1.65031×10^{14}	1.97037×10^{14}	0.837565
	1	1.66744×10^{14}	1.27032×10^{18}	1.31261×10^{-4}

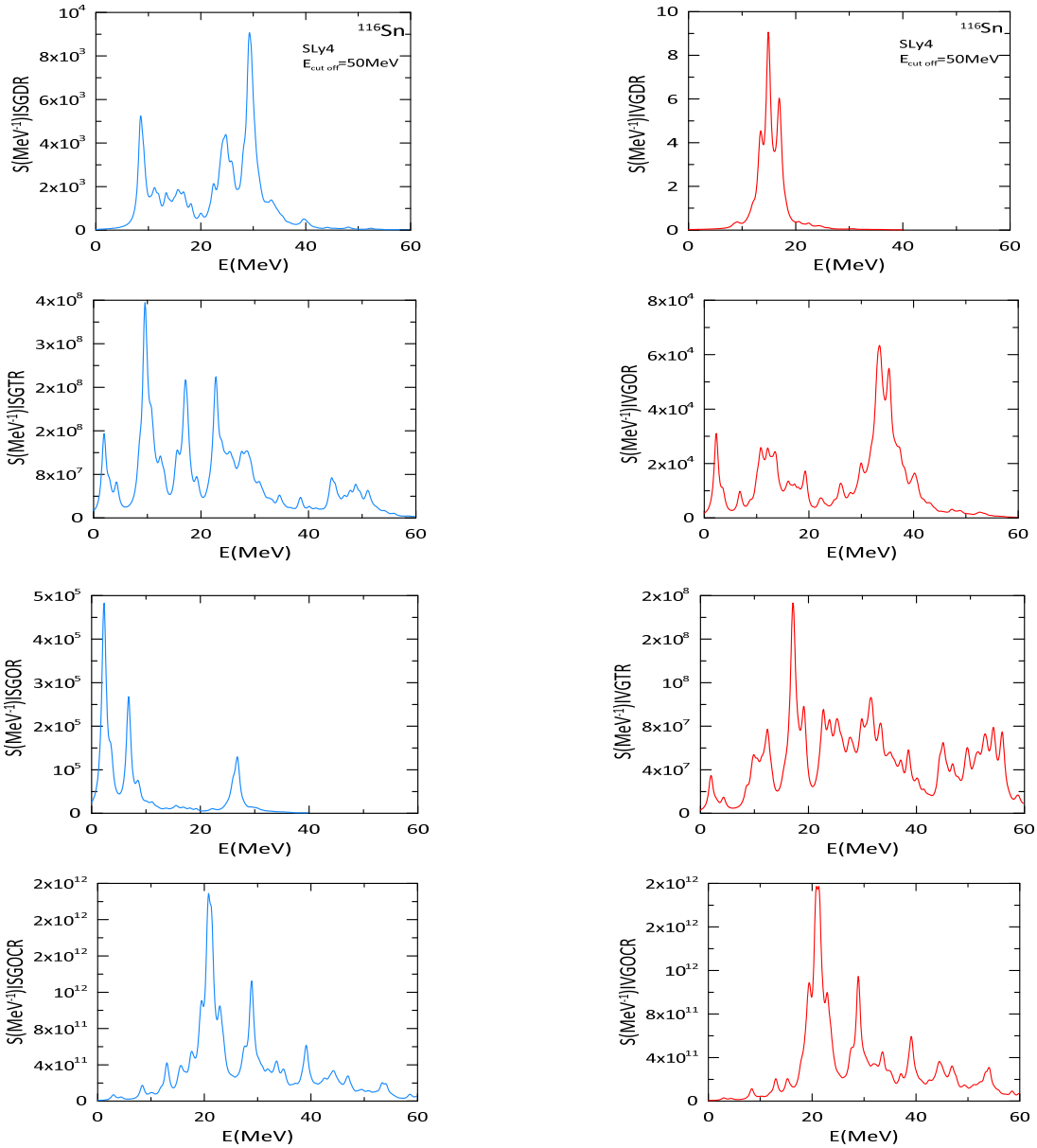

Figure 15. IS (left panel) as well as IV (right panel) HF-based RPA strength function for the dipole photo absorption cross section (E1), octopole (E3), triacontadipole (E5), and octacosahectapole (E7) in ^{116}Sn, using the SLy4 Skyrme interaction

Table 8. The same as Table 7, for ^{116}Sn. The results are obtained by using the SLy4 parameterization.

J^{π}	T	m1 (RPA)	m1(D.C)	R
1^-	0	1.58971×10^{6}	1.60455×10^{6}	0.9907
	1	4.95137×10^{2}	4.98954×10^{2}	0.9923
3^-	0	1.67417×10^{7}	1.68763×10^{7}	0.9920
	1	1.84779×10^{7}	1.86690×10^{7}	0.9897
5^-	0	9.05465×10^{10}	9.30575×10^{10}	0.9730
	1	9.46386×10^{10}	9.80651×10^{10}	0.9650
7^-	0	5.76248×10^{14}	6.39154×10^{14}	0.9015
	1	5.83076×10^{14}	6.21586×10^{18}	9.3804×10^{-5}

Table 9. The same as Table 8, for ^{144}Sm. The results are obtained by using the SLy5 parameterization.

J^{π}	T	m1 (RPA)	m1(D.C)	R
5^-	0	1.7375×10^{11}	1.74605×10^{11}	0.9951
	1	1.83920×10^{11}	1.85616×10^{11}	0.9908
7^-	0	1.11146×10^{15}	1.24269×10^{15}	0.8943
	1	1.13293×10^{15}	1.70570×10^{19}	6.6420×10^{-5}

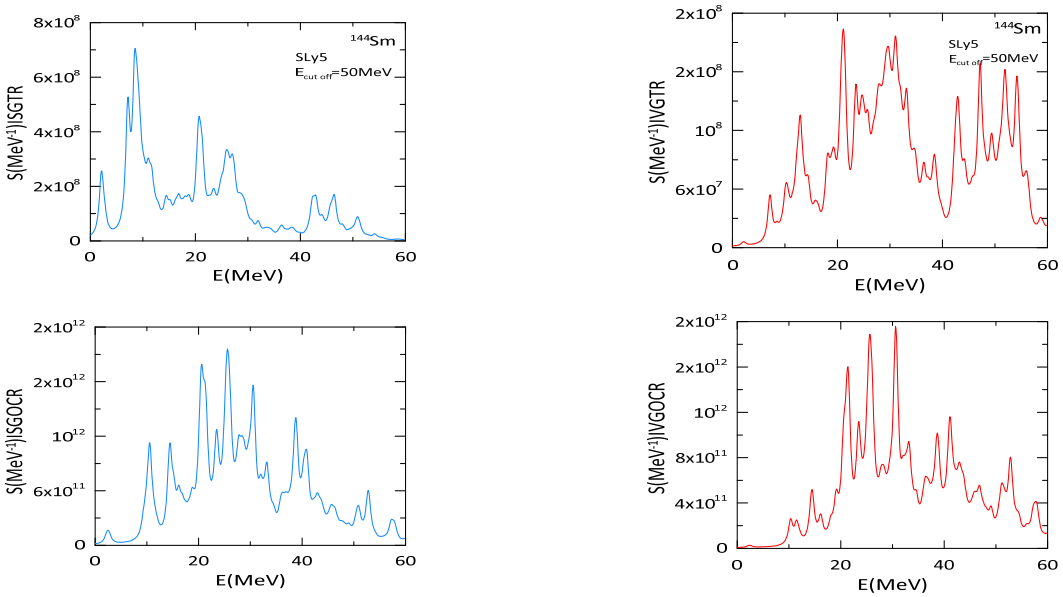

Figure16. IS (left panel) as well as IV (right panel) HF-based RPA strength function for the triacontadipole (E5), and octacosahectapole (E7) in ^{144}Sm, using the SLy5 Skyrme interaction

CONCLUSIONS

The present research has led us to conclude that self-consistent RPA calculations are based on Skyrme effective nucleon-nucleon interaction, and these calculations give a significant description of the ground state properties for the closed-shell for ^{58}Ni, ^{90}Zr, ^{116}Sn, and ^{144}Sm. Considering the binding energy, neutron, proton, and neutron skin thickness, and charge radii, remarkable correlations were found with experimental data. For the static nuclear properties, the SLy4 and SLy5 parameterizations give the best results in compression with experimental data. Regarding dynamic properties, the RPA method is an efficient tool for describing the higher modes resulting from the collective motion of nucleons within the nucleus. It can also be used to describe the transition. density for proton· and neutron modes, in addition to GRs modes. The RPA method is the simplest theory that predicts the main features of giant resonance (GR) with a high degree of accuracy.

Competing interests. The authors did not receive support from any organization for the submitted work.

ORCID IDs

Noor M. Kareem, https://orcid.org/0000-0002-2275-9398; **Ali A. Alzubadi,** https://orcid.org/0000-0002-7226-1141

REFERENCES

[1] A.L. Fetter, and J.D. Walecka, *Quantum Theory of Many-Particle Systems*, (Dover Publications, Mineola, NY, 2003).
[2] J.W. Negele, "The mean-field theory of nuclear structure and dynamics," Rev. Mod. Phys. **54**(4), 913 (1982). https://doi.org/10.1103/RevModPhys.54.913
[3] M. Bender, P.-H. Heenen, and P.-G. Reinhard, "Self-consistent mean-field models for nuclear structure," Rev. Mod. Phys. **75**(1), 121 (2003). https://doi.org/10.1103/RevModPhys.75.121
[4] J.R. Stone, and P.G. Reinhard, Prog. Part. Nucl. Phys. **58**(2), 587 (2007). https://doi.org/10.1016/j.ppnp.2006.07.001
[5] K.S. Krane, *Introductory Nuclear Physics*, 3rd ed. (John Wiley Sons, New York, 1987).
[6] A.A. Alzubadi, A.J. Alhaideri, and N.F. Lattoofi, "Study of static and dynamic properties of even-even 14–24O and 38–54Ca in the frame of Random Phase Approximation (RPA) method with different Skyrme parameterizations," Phys. Scr. **96**(5), 55304 (2021). https://doi.org/10.1088/1402-4896/abe9f0
[7] S.S.M. Wong, *Introductory nuclear physics*, (John Wiley & Sons, 2008).
[8] W. Greiner, and J.A. Maruhn, *Nuclear models*, (Springer, 1996).
[9] D.R. Hartree, "The wave mechanics of an atom with a non-Coulomb central field. Part I. Theory and methods," in: *Mathematical Proceedings of the Cambridge Philosophical Society*, 24(1), 1928, pp. 89-110, (Cambridge University Press, 2008). https://doi.org/10.1017/S0305004100011919
[10] G. Co', and S. De Leo, "Hartree–Fock and random phase approximation theories in a many-fermion solvable model," Mod. Phys. Lett. A, **30**(36), 1550196 (2015). https://doi.org/10.1142/S0217732315501965
[11] E.B. Suckling, Ph.D. dissertation, The University of Surrey, March 2011.
[12] D. Vautherin, and D.M. Brink, "Hartree-Fock calculations with Skyrme's interaction," Phys. Lett. B, **32**(3), 149 (1970). https://doi.org/10.1016/0370-2693(70)90458-2
[13] B.A. Brown, S.E. Massen, and P.E. Hodgson, "Proton and neutron density distributions for A= 16-58 nuclei," J. Phys. G. Nucl. Phys. **5**(12), 1655 (1979). https://doi.org/10.1088/0305-4616/5/12/008
[14] T.H.R. Skyrme, "The effective nuclear potential," Nucl. Phys. **9**(4), 615 (1958). https://doi.org/10.1016/0029-5582(58)90345-6

[15] E. Chabanat, P. Bonche, P. Haensel, J. Meyer, and R. Schaeffer, "A Skyrmeparametrization from subnuclear to neutron star densities Part II. Nuclei far from stabilities," Nucl. Phys. A, **635**(1-2), 231 (1998). https://doi.org/10.1016/S0375-9474(98)00180-8
[16] K.L.G. Heyde, "The nuclear shell model," in: *The Nuclear Shell Model*, (Springer, Berlin, Heidelberg, 1994), pp. 58-154. https://doi.org/10.1007/978-3-642-79052-2_4
[17] D. Vautherin, and D.M.T. Brink, "Hartree-Fock calculations with Skyrme's interaction. I. Spherical nuclei," Phys. Rev. C, **5**(3), 626 (1972). https://doi.org/10.1103/PhysRevC.5.626
[18] D.J. Rowe, *Nuclear Collective Motion*, (Methuen and Co, Ltd., London, 1970), vol. 211.
[19] P. Sarriguren, E.M. de Guerra, and R. Nojarov, "Spin M1 excitations in deformed nuclei from self-consistent Hartree-Fock plus random-phase approximation," Phys. Rev. C, **54**(2), 690 (1996). https://doi.org/10.1103/PhysRevC.54.690
[20] H. Nakada, "Mean-field and RPA approaches to stable and unstable nuclei with semi-realistic NN interactions," in Journal of Physics: Conference Series, **445**(1), 012011 (2013). https://doi.org/10.1088/1742-6596/445/1/012011
[21] P.J. Brussaard, and P.W.M. Glaudemans, *Shell-model applications in nuclear spectroscopy*, (North-Holland publishing company, 1977).
[22] P. Ring, and P. Schuck, *Problems of many bodies*, (Springer-Verlag, New York, 1980).
[23] D.R. de Oliveira, "The Hartree-Fock and the random phase approximations applied to Ne^{20}, Si^{28} and Ar^{36}: Energy Levels and E2 Transition" Rev. Bras. Física, **1**(3), 403 (1971).
[24] B.A. Brown, *Lecture notes in nuclear structure physics*, Natl. Super Conduct. Cyclotr. Lab. (2005).https://people.nscl.msu.edu/~brown/reaction-codes/wspot/wspot-brown.pdf
[25] I. Angeli, and K.P. Marinova, "Table of experimental nuclear ground state charge radii: An update," At. Data Nucl. Data Tables, **99**(1), 69 (2013). https://doi.org/10.1016/j.adt.2011.12.006
[26] Lomonosov Moscow State University, Skobeltsyn Institute Of Nuclear Physics, CenterDannykhFotoyadernykhExperimentov, http://cdfe.sinp.msu.ru/services/
[27] H. De Vries, C.W. De Jager, and C. De Vries, "Nuclear charge-density-distribution parameters from elastic electron scattering," At. Data Nucl. Data Tables, **36**(3), 495 (1987). https://doi.org/10.1016/0092-640X(87)90013-1
[28] Myanmar Education Research and Learning Portal, H.M. Thandar, and K.S. Myint, "Calculation of Form Factor for ^{116}Sn and^{118}Sn by Using Three-Parameter Gaussian Model Density Distribution." https://meral.edu.mm/records/5559
[29] S. Goriely, S. Hilaire, M. Girod, and S. Péru, "First Gogny-Hartree-Fock-Bogoliubov nuclear mass model," Phys. Rev. Lett. **102**(24), 242501 (2009). https://doi.org/10.1103/PhysRevLett.102.242501
[30] B.K. Agrawal, S. Shlomo, and A.I. Sanzhur, "Self-consistent Hartree-Fock based random phase approximation and the spurious state mixing," Phys. Rev. C, **67**(3), 034314 (2003). https://doi.org/10.1103/PhysRevC.67.034314
[31] P.-G. Reinhard, D.J. Dean, W. Nazarewicz, J. Dobaczewski, J.A. Maruhn, and M. R. Strayer, "Shape coexistence and the effective nucleon-nucleon interaction," Phys. Rev. C, **60**(1), 14316 (1999). https://doi.org/10.1103/PhysRevC.60.014316
[32] P. Chomaz and N. Frascaria, "Multiple phonon excitation in nuclei," P00020240, 1993. https://cds.cern.ch/record/257796/files/P00020240.pdf
[33] International Atomic Energy Agency - Nuclear Data Section. Vienna International Centre, Vienna, Austria. https://www-nds.iaea.org/

ДОСЛІДЖЕННЯ ЯДЕРНОЇ СТРУКТУРИ ДЕЯКИХ ЯДЕР ЗА ДОПОМОГОЮ САМОУЗГОДЖЕНИХ РОЗРАХУНКІВ RPA ІЗ ВЗАЄМОДІЄЮ ТИПУ SKYRME

Нур М. Карім[a], Алі А. Алзубаді[a]
[a]Університет Багдада, Науковий коледж, факультет фізики

У цьому дослідженні були вивчені деякі статичні та динамічні ядерні властивості ядер із закритою оболонкою:^{58}Ni, ^{90}Zr, ^{116}Sn і ^{144}Sm з використанням методу Random Phase Approximation (RPA) і різних параметрів Скірма, зокрема SyO-, Sk255, SyO+, SLy4, BSk17 і SLy5. Зокрема, у дослідженнях статичних властивостей, таких як ядерна густина для нейтронів, протонів, маса та густина заряду з їхніми відповідними середньоквадратичними радіусами, одночастинкові розподіли ядерної густини. Усі отримані результати добре узгоджуються з відповідними експериментальними даними. Що стосується динамічних властивостей, також були вивчені енергія збудження, щільність переходу та гігантські резонансні моди для збудження низькорозташованих негативних збуджених станів 1^-, 3^-, 5^- та 7^-. Результати показують, що оцінки RPA з взаємодіями типу Skyrme є хорошим способом опису властивостей структури парно-парних ядер із закритою оболонкою.

Ключові слова:сили SKYRME, Хартрі-Фок (HF), апроксимація випадкової фази (RPA), збуджений стан вищих мод, щільність енергії Skyrme